



*Supplement of*

## **Role of K-feldspar and quartz in global ice nucleation by mineral dust in mixed-phase clouds**

**Marios Chatziparaschos et al.**

*Correspondence to:* Maria Kanakidou (mariak@uoc.gr)

The copyright of individual parts of the supplement might differ from the article licence.

## **Methodology to derive the dust content of atmospheric aerosols.**

Air masses from Africa transported over the open sea were selectively sampled at Miami and Barbados stations. The mineral dust fraction was then calculated from the aluminium (Al) content in the ash residue of the burned sample (assuming an 8% Al content) (Zuidema et al., 2019). At the location of Cayenne, the dust load is calculated by subtracting a regional background 5 from the PM<sub>10</sub> concentrations measured by the ATMO-Guyane organizations using TEOM (tapered element oscillating microbalance) instrumentation (Prospero et al., 2020). For the Sahel stations, the reported measurements are for total PM<sub>10</sub>. As the stations lie close to the dust emission source, dust concentration can be estimated by omitting in the calculation of the monthly averages the air masses originating from areas containing a significant amount of aerosols from other sources (mainly, biomass burning for Banizoumbou and Cinzana, sea salt and urban pollution for M'Bour and Bambey) (Reid et al., 005; Lebel 10 et al., 2010; Kok et al., 2021). Filtering the observations according to wind direction might lead, however, to an overestimation of the real dust concentrations, as even dust-rich air masses coming from the source regions may contain aerosols other than dust. For the stations of Banizoumbou (Niger, 13.54°N, 2.66°E) and Cinzana (Mali, 13.28°N, 5.93°W), we filtered out southerly air masses during the dry season (December to February) to avoid the interference of biomass burning aerosols (Cavalieri et al., 2010). For the M'Bour (Senegal, 14.39°N, 16.96°W) and Bambey (Senegal, 14.70 °N, 16.47 °W) stations, we 15 excluded the air masses rich in sea-salt and pollutants associated with wind sectors originating from marine and urban areas. Following Kok et al. (2021), we accounted for the correction from geometric to aerodynamic diameter when comparing the model dust concentration with the Sahel measurements. To do so, we used the result of Huang et al. (2020), who calculated that for desert dust, a geometric diameter of 6.8 μm corresponds to an aerodynamic diameter of 10 μm. For the stations of Agia Marina (35°N, 33.06°E) (Pikridas et al., 2018) and Finokalia (25.67°N, 35.34°E), the dust concentration is calculated 20 from measurements of total PM load following the methodology developed by Escudero et al. (2007) using air mass origin characterization based on air mass back-trajectories.

## **Equations used for the statistical analysis**

Mathematical formulas for correlation coefficient (R; Eq. S1), normalized mean bias (nMB; Eq. S2), and the normalized root 25 mean square error (nRMSE; Eq. S3) that used for the statistical analysis between model observations; O<sub>i</sub> and P<sub>i</sub> stand for observations and predictions respectively and also N is the number of pairs (observations, predictions) that are compared.

$$R = \left[ \frac{\frac{1}{N} \sum_{i=1}^N (O_i - \bar{O})(P_i - \bar{P})}{\sigma_O \sigma_P} \right] \quad (\text{Eq.S1})$$

$$30 \quad NMB = \frac{\sum_{i=1}^N (M_i - O_i)}{\sum_{i=1}^N (O_i)} \times 100 \quad (\text{Eq.S2})$$

$$nRMSE = \frac{\sqrt{\frac{1}{N} \sum_{i=1}^N (P_i - O_i)^2}}{\sum_{i=1}^N O_i} \quad (\text{Eq.S3})$$

## 35 Supplementary figures

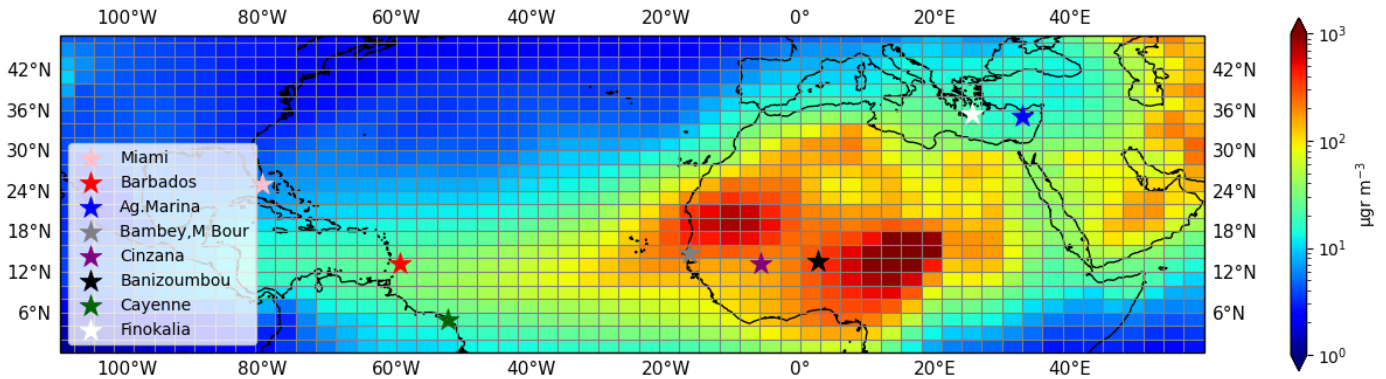


**Figure S1:** The location of the 8 stations used for the model validation, plotted over the dust concentration field simulated by TM4-ECPL model for summer 2015. Note that the two stations, M'Bour and Bambeay, are so close to each other that they are superimposed on the map.

40 The grey grids correspond to the model gridding in  $3^\circ \times 2^\circ$  resolution.

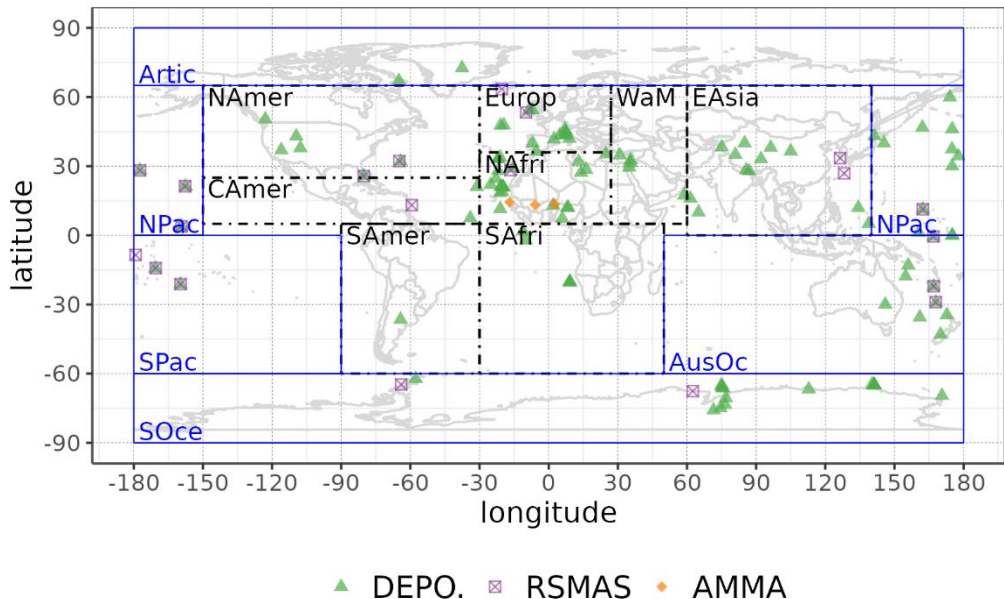
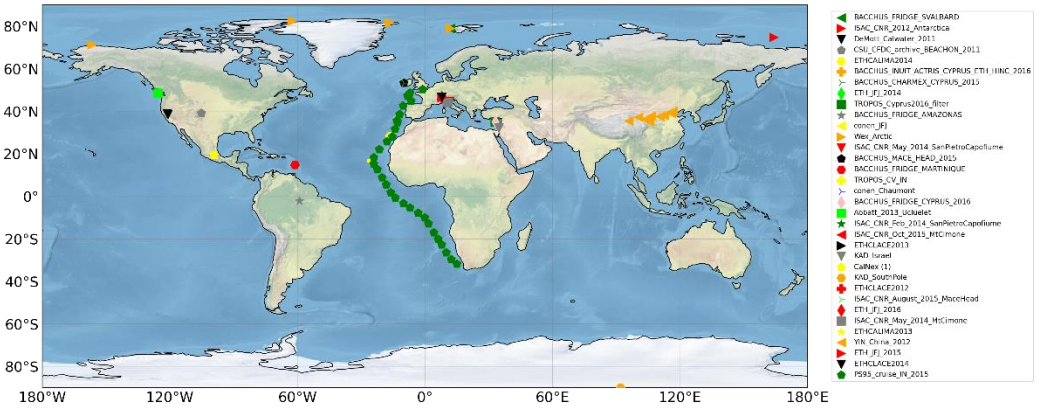
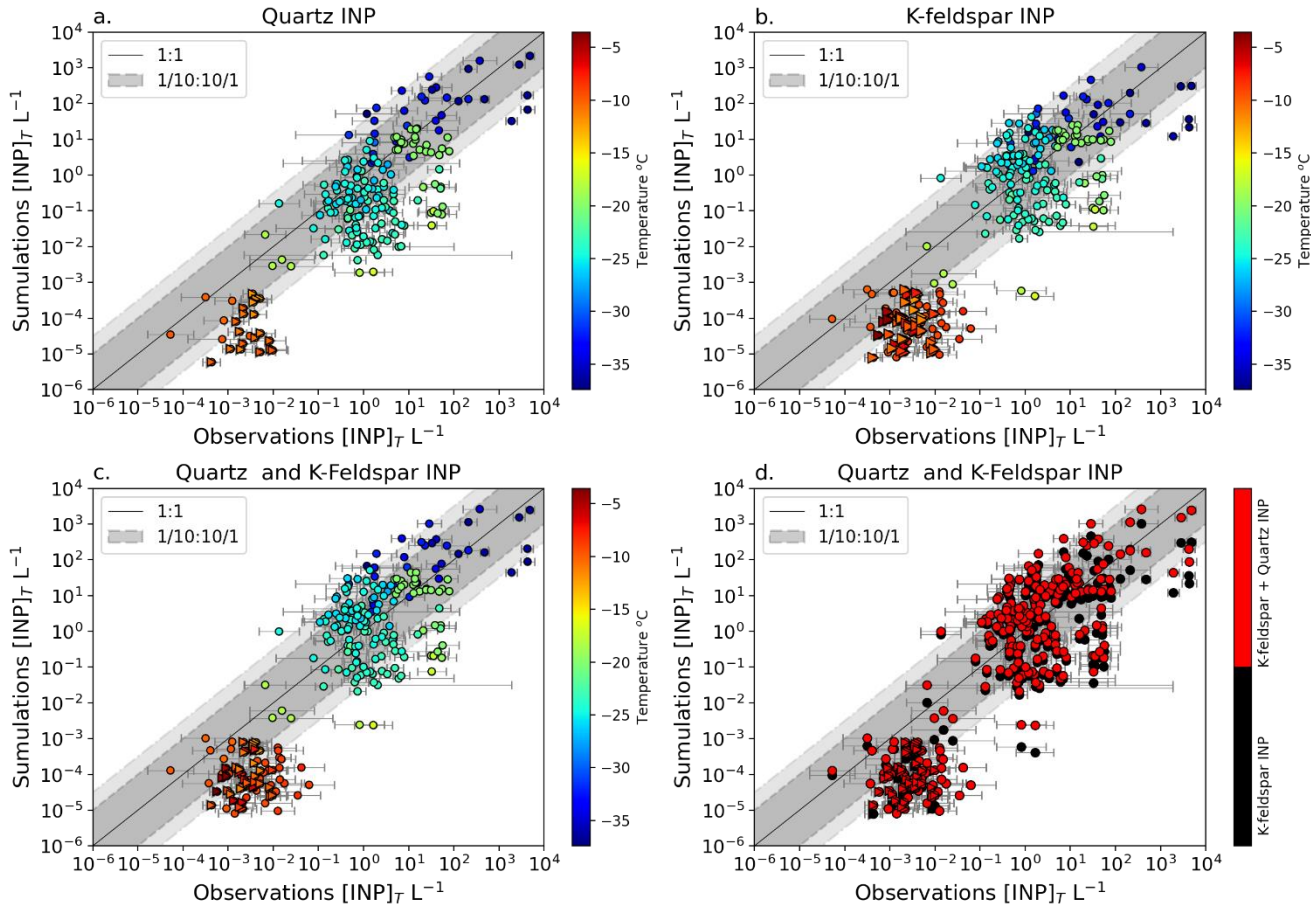


**Figure S2:** Site location map of observations dust surface concentration (RSMAS, purple squares; AMMA, orange diamonds), and dust deposition rates (several sources compiled in Albani et al., 2014, green triangles).



45

**Figure S3:** Location of the data used for comparison in Figure 4. The name of the campaigns for these datasets, the locations and the corresponding literature references are provided in Table S3.



50

**Figure S4:** Comparison of [INP]<sub>T</sub> concentrations calculated at the temperature of the measurements against observations (dates and locations provided in the supplementary Table S1). (a) simulating only quartz derived INP, (b) simulating only K-feldspar derived INP and (c) simulating both quartz and K-feldspar derived INP (d) simulating only feldspar INP (black circles) and both quartz and K-feldspar INP (red circles). This figure is related to Fig 4.

55

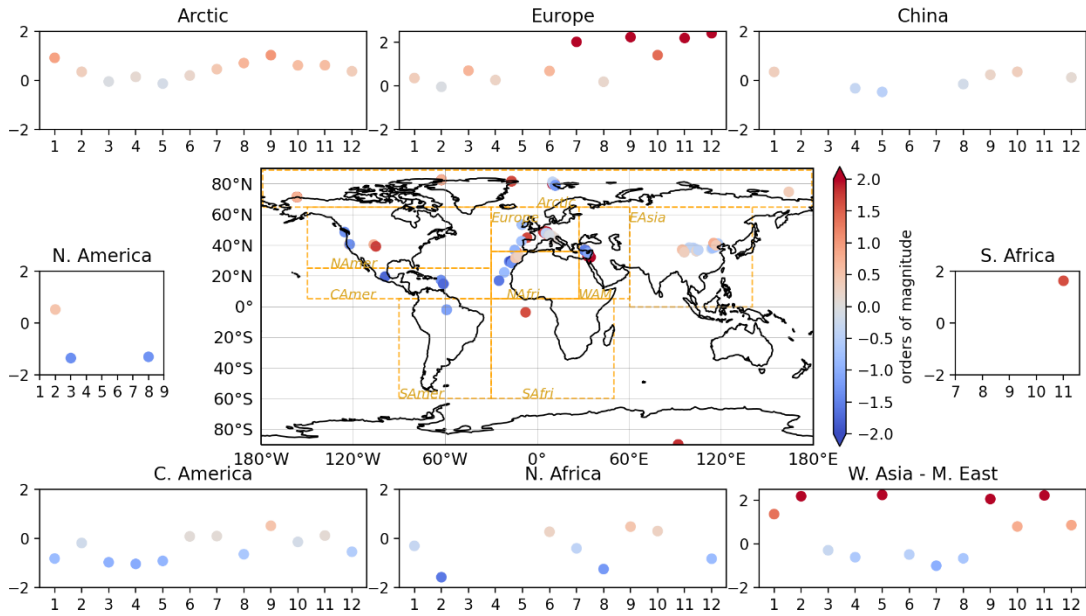
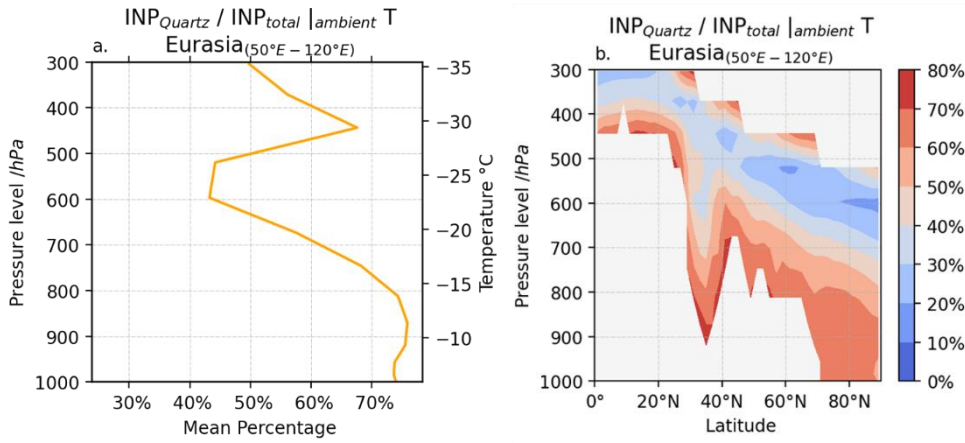


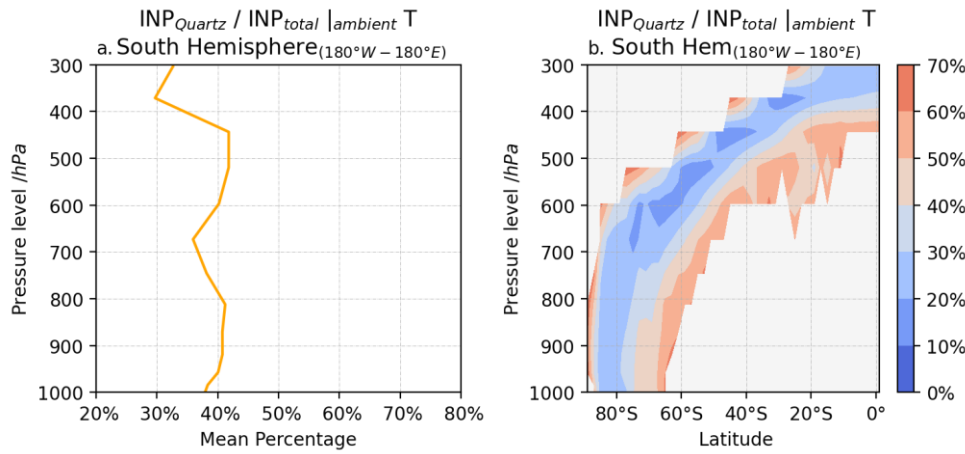
**Figure S5:** Shows the locations where model overestimates (blueish) and underestimates (reddish) INP observations by  $\pm 2$  orders of magnitude (colour-bar). The location of the points with same coordinates have been moved randomly (1-4° degrees) in the plot for purpose of visualization so it can be seen when the bias affects a single data point. The plots surrounding the map show the climatological monthly mean of the deviations between modelled and observed INP concentration for specific regions. Y-axis shows the bias between model results and observations calculated as the difference  $\log_{10}(\text{observations}) - \log_{10}(\text{model})$  while the x-axis indicates the corresponding month or the year.

60

65



70 **Figure S6:** (a) Profile of the mean percent contribution of INP from quartz minerals over Eurasia. (b) Annual zonal mean over Eurasia. this figure is related with Fig 7.



75 **Figure S7:** (a) Profile of mean percent contribution of INP from quartz minerals in the South Hemisphere. (b) Annual zonal mean of the percent contribution of INP<sub>quartz</sub> to the total INP from dust in the South Hemisphere. This figure is related to Fig 8.

## Supplementary tables

**Table S1:** Summary of statistics for all points and per region for the evaluation of (a) the modelled annual mean dust surface concentration for 2009– 2016 compared to climatological mean values from RSMAS sites and AMMA campaign, and (b) the modelled annual dust deposition flux averaged for the same period against observations as compiled in Albani et al. (2014) from several sources. The number of stations (n), the Pearson correlation coefficients (R) between the simulated and measured monthly mean concentrations, the normalized mean bias (nMB), and the normalized root-mean-square errors (nRMSEs) are indicated for the TM4-ECPL simulation.

	n	R	nMB(%)	nRMSE (%)
<b>Dust surface concentration</b>				
N. America	1		35.66	38.54
C. America	2		50.60	50.60
Europe	2		-48.92	88.03
N. Africa	4		37.97	66.62
E. Asia	2		138.61	150.95
Australian oceans	3		87.83	111.26
S. Pacific Ocean	3		105.04	115.32
N. Pacific Ocean	4		630.89	803.67
Southern Ocean	2		-48.25	61.84
All Points	23	<b>0.93</b>	44.10	143.20
<b>Dust Deposition rates</b>				
Arctic	2		1032.05	1038.09
N. America	6		-83.42	107.81
C. America	2		-44.25	68.06
S. America	1		-99.35	99.35
Europe	13		-74.28	129.73
N. Africa	23		-54.33	143.07
S. Africa	5		-77.39	92.66
W. Asia and M. East	5		-94.72	163.86
E. Asia	12		-31.93	190.09
Australian oceans	9		-94.62	195.95
S. Pacific Ocean	2		-60.99	63.05
N. Pacific Ocean	15		-30.02	79.72
Southern Ocean	15		1290.20	1475.04
All Points	110	<b>0.8</b>	-59.20	233.40

**Table S2:** Statistical performance of the different minerals. Pt1 and Pt1.5 are the percentages of data points reproduced within an order of magnitude and 1.5 orders of magnitude in the temperature range of every parameterization. R\_1 and R\_1.5 are the correlation coefficient correspond the related Pt1 and Pt1.5 percentages. The number of data points used for calculating these values is shown under the data points column. The correlation coefficient has been calculated with the logarithm of the values.

Parameterization: (Harrison et al., 2019)	Temperature range	Pt_1	R_1	Data point	Pt_1.5	R_1.5	Data points	R
Quartz	-10.5 to -37.5 °C	45%	0.74	119	58%	0.63	153	
K-feldspar	-3.5 to -37.5 °C	50%	0.93	132	66%	0.91	172	
K-feldspar and quartz		51%	0.94	135	69%	0.92	181	
All points							263	0.84

**Table S3:** Data sets used for this study. Campaign/data

Campaign/data set	Location	References
Arctic station Barrow/Utqiagvik	Arctic	(Wex et al., 2019)
Alert (Canadian Arctic Station)	Arctic	
Arctic station Ny-Ålesund	Arctic	
Station_Nord (Villum Research Station)	Arctic	
PS95 Atlantic Cruise 2015	Atlantic	(Welti et al., 2020)
KAD_Israel	Tel Aviv	(Ardon-Dryer and Levin, 2014)
KAD_South_Pole	South Pole	(Ardon-Dryer et al., 2011)
Conen_Chaumont	Jungfraujoch and Chaumont	(Conen et al., 2015)
CYPRUS BACCHUS/CHARMEX 2015	Forestry Department site, Agia Marina	(Ansmann et al., 2019)
BACCHUS_FRIDGE	Amazonian Tall Tower Observatory	(Schrod et al., 2020)
AMAZONAS		
CalWater	Coastal California, Airborne	(Fan et al., 2014)
Conen_JFJ	Jungfraujoch	(Conen et al., 2015)
CLACE2014	Jungfraujoch	
CLACE2013	Jungfraujoch	(Lacher et al., 2021, 2018, 2017)
CLACE2012	Jungfraujoch	(Boose et al., 2016)
CallNex	California	(Wang et al., 2012)
CALIMA 2014	Izana observatory, Tenerife	(Boose et al., 2016)
CALIMA 2013	Izana observatory, Tenerife	(Boose et al., 2016)
ISAC-CNR MaceHead	Mace Head Observatory, Carna, Galway, Ireland	(Rinaldi et al., 2016)
BACCHUS Campaign		

<i>ISAC-CNR SanPietro_Capofiume</i>	San Pietro	(Belosi et al., 2017)
<i>BACCHUS Campaign</i>	Capofiume (BO, Italy)	
<i>ISAC_CNR_MtCimone</i>	mountain	(Rinaldi et al., 2017)
<i>BACCHUS Campaign</i>	observatory Mt. Cimone	
<i>ISAC-CNR Antarctica</i>	Mario Zucchelli	(Belosi et al., 2014)
<i>BACCHUS Campaign</i>	Station, Terranova Bay, Antarctica	
<i>BACCHUS_FRIDGE_SVALBARD</i>	Zeppelin	(Schrod et al., 2020)
<i>Campaign</i>	Observatory, Svalbard/Spitzberg en	
<i>BACCHUS_FRIDGE_MARTINIQUE</i>	Volcanic and Seismologic Observatory, Fonds-Saint-Denis, Martinique, Caribbean	(Schrod et al., 2020)
<i>CSU_CFDC_archive_BEACHON</i>	Manitou	(Tobo et al., 2013)
<i>ETH_JFJ_2014</i>	Experimental ForestObservatory (MEFO)	
	Jungfraujoch High Altitude Research Station	(Lacher et al., 2017)
<i>ETH_JFJ_2016</i>	Jungfraujoch High Altitude Research Station	(Lacher et al., 2017, 2018)
<i>ETH_JFJ_2015</i>	Jungfraujoch High Altitude Research Station	(Lacher et al., 2017)
<i>TROPOS_Cyprus2016</i>	Agia Marina, Xyliatou, Cyprus	(Ansmann et al., 2019; Schrod et al., 2017)
<i>TROPOS_CV_IN</i>	Cape Verde	(Welti et al., 2018)
<i>Yin_China</i>	China	(Yin et al., 2012)
<i>NETCARE_2013</i>	Coastal (West coast of Canada)	(Mason et al., 2015)

## References

- Ansmann, A., Mamouri, R. E., Bühl, J., Seifert, P., Engelmann, R., Hofer, J., Nisantzi, A., Atkinson, J. D., Kanji, Z. A., Sierau, B., Vrekoussis, M., and Sciare, J.: Ice-nucleating particle versus ice crystal number concentration in 100 altocumulus and cirrus layers embedded in Saharan dust:a closure study, *Atmos. Chem. Phys.*, 19, 15087–15115, <https://doi.org/10.5194/acp-19-15087-2019>, 2019.
- Ardon-Dryer, K. and Levin, Z.: Ground-based measurements of immersion freezing in the eastern Mediterranean, *Atmos. Chem. Phys.*, 14, 5217–5231, <https://doi.org/10.5194/acp-14-5217-2014>, 2014.
- Ardon-Dryer, K., Levin, Z., and Lawson, R. P.: Characteristics of immersion freezing nuclei at the South Pole 105 station in Antarctica, *Atmos. Chem. Phys.*, 11, 4015–4024, <https://doi.org/10.5194/acp-11-4015-2011>, 2011.
- Belosi, F., Santachiara, G., and Prodi, F.: Ice-forming nuclei in Antarctica: New and past measurements, *Atmos. Res.*, 145–146, 105–111, <https://doi.org/10.1016/j.atmosres.2014.03.030>, 2014.

- Belosi, F., Rinaldi, M., Decesari, S., Tarozzi, L., Nicosia, A., and Santachiara, G.: Ground level ice nuclei particle measurements including Saharan dust events at a Po Valley rural site (San Pietro Capofiume, Italy),  
110 *Atmos. Res.*, 186, 116–126, <https://doi.org/10.1016/j.atmosres.2016.11.012>, 2017.
- Boose, Y., Sierau, B., Isabel García, M., Rodríguez, S., Alastuey, A., Linke, C., Schnaiter, M., Kupiszewski, P., Kanji, Z. A., and Lohmann, U.: Ice nucleating particles in the Saharan Air Layer, *Atmos. Chem. Phys.*, 16, 9067–9087, <https://doi.org/10.5194/acp-16-9067-2016>, 2016.
- Cavalieri, O., Cairo, F., Fierli, F., Di Donfrancesco, G., Snels, M., Viterbini, M., Cardillo, F., Chatenet, B.,  
115 Formenti, P., Marticorena, B., and Rajot, J. L.: Variability of aerosol vertical distribution in the Sahel, *Atmos. Chem. Phys.*, 10, 12005–12023, <https://doi.org/10.5194/acp-10-12005-2010>, 2010.
- Conen, F., Rodríguez, S., Hüglin, C., Henne, S., Herrmann, E., Bukowiecki, N., and Alewell, C.: Atmospheric ice nuclei at the high-altitude observatory Jungfraujoch, Switzerland, *Tellus, Ser. B Chem. Phys. Meteorol.*, 67,  
<https://doi.org/10.3402/tellusb.v67.25014>, 2015.
- 120 Escudero, M., Querol, X., Pey, J., Alastuey, A., Pérez, N., Ferreira, F., Alonso, S., Rodríguez, S., and Cuevas, E.: A methodology for the quantification of the net African dust load in air quality monitoring networks, *Atmos. Environ.*, 41, 5516–5524, <https://doi.org/10.1016/j.atmosenv.2007.04.047>, 2007.
- Fan, J., Leung, L. R., Demott, P. J., Comstock, J. M., Singh, B., Rosenfeld, D., Tomlinson, J. M., White, A.,  
125 Prather, K. A., Minnis, P., Ayers, J. K., and Min, Q.: Aerosol impacts on California winter clouds and precipitation during calwater 2011: Local pollution versus long-range transported dust, *Atmos. Chem. Phys.*, 14, 81–101, <https://doi.org/10.5194/acp-14-81-2014>, 2014.
- Huang, Y., Kok, J. F., Kandler, K., Lindqvist, H., Nousiainen, T., Sakai, T., Adebiyi, A., and Jokinen, O.: Climate Models and Remote Sensing Retrievals Neglect Substantial Desert Dust Asphericity, *Geophys. Res. Lett.*, 47, 1–11, <https://doi.org/10.1029/2019GL086592>, 2020.
- 130 Kok, J. F., Adebiyi, A. A., Albani, S., Balkanski, Y., Checa-Garcia, R., Chin, M., Colarco, P. R., Hamilton, D. S., Huang, Y., Ito, A., Klose, M., Leung, D. M., Li, L., Mahowald, N. M., Miller, R. L., Obiso, V., Pérez García-Pando, C., Rocha-Lima, A., Wan, J. S., and Whicker, C. A.: Improved representation of the global dust cycle using observational constraints on dust properties and abundance, *Atmos. Chem. Phys.*, 21, 8127–8167, <https://doi.org/10.5194/acp-21-8127-2021>, 2021.
- 135 Lacher, L., Lohmann, U., Boose, Y., Zipori, A., Herrmann, E., Bukowiecki, N., Steinbacher, M., and Kanji, Z. A.: The Horizontal Ice Nucleation Chamber HINC: INP measurements at Conditions Relevant for Mixed-Phase Clouds at the High Altitude Research Station Jungfraujoch, *Atmos. Chem. Phys. Discuss.*, 1–49, <https://doi.org/10.5194/acp-2017-474>, 2017.
- Lacher, L., DeMott, P. J., Levin, E. J. T., Suski, K. J., Boose, Y., Zipori, A., Herrmann, E., Bukowiecki, N.,  
140 Steinbacher, M., Gute, E., Abbatt, J. P. D., Lohmann, U., and Kanji, Z. A.: Background Free-Tropospheric Ice Nucleating Particle Concentrations at Mixed-Phase Cloud Conditions, *J. Geophys. Res. Atmos.*, 123, 10,506–10,525, <https://doi.org/10.1029/2018JD028338>, 2018.
- Lacher, L., Clemen, H. C., Shen, X., Mertes, S., Gysel-Beer, M., Moallemi, A., Steinbacher, M., Henne, S.,  
145 Saathoff, H., Mohler, O., Hohler, K., Schiebel, T., Weber, D., Schrod, J., Schneider, J., and Kanji, Z. A.: Sources and nature of ice-nucleating particles in the free troposphere at Jungfraujoch in winter 2017, *Atmos. Chem. Phys.*, 21, 16925–16953, <https://doi.org/10.5194/acp-21-16925-2021>, 2021.
- Lebel, T., Parker, D. J., Flamant, C., Bourlès, B., Marticorena, B., Mougin, E., Peugeot, C., Diedhiou, A., Haywood, J. M., Ngamini, J. B., Polcher, J., Redelsperger, J. L., and Thorncroft, C. D.: The AMMA field campaigns: Multiscale and multidisciplinary observations in the West African region, *Q. J. R. Meteorol. Soc.*, 150 136, 8–33, <https://doi.org/10.1002/qj.486>, 2010.
- Mason, R. H., Si, M., Li, J., Chou, C., Dickie, R., Toom-Sauntry, D., Pöhlker, C., Yakobi-Hancock, J. D.,  
Ladino, L. A., Jones, K., Leaitch, W. R., Schiller, C. L., Abbatt, J. P. D., Huffman, J. A., and Bertram, A. K.: Ice nucleating particles at a coastal marine boundary layer site: Correlations with aerosol type and meteorological conditions, *Atmos. Chem. Phys.*, 15, 12547–12566, <https://doi.org/10.5194/acp-15-12547-2015>, 2015.
- 155 Pikridas, M., Vrekoussis, M., Sciare, J., Kleanthous, S., Vasiliadou, E., Kizas, C., Savvides, C., and

Mihalopoulos, N.: Spatial and temporal (short and long-term) variability of submicron, fine and sub-10 Mm particulate matter (PM1, PM2.5, PM10) in Cyprus, *Atmos. Environ.*, 191, 79–93, <https://doi.org/10.1016/j.atmosenv.2018.07.048>, 2018.

Prospero, J. M., Barkley, A. E., Gaston, C. J., Gatineau, A., Campos y Sansano, A., and Panechou, K.: Characterizing and Quantifying African Dust Transport and Deposition to South America: Implications for the Phosphorus Budget in the Amazon Basin, *Global Biogeochem. Cycles*, 34, 1–24, <https://doi.org/10.1029/2020GB006536>, 2020.

Reid, J. S., Eck, T. F., Christopher, S. A., Koppman, R., Dubovik, O., Eleuterio, D. P., Holben, B. N., Reid, E. A., and Zhang, J.: A review of biomass burning emissions part III: Intensive optical properties of biomass burning particles, *Atmos. Chem. Phys.*, 5, 827–849, <https://doi.org/10.5194/acp-5-827-2005>, 2005.

Rinaldi, M., Belosi, F., Nicosia, A., Santachiara, G., Decesari, S., and Cristina, M.: Ice Nucleating Particles at Mace Head during the 2015 BACCHUS campaign through off-line measurements, 18, 15063, 2016.

Rinaldi, M., Santachiara, G., Nicosia, A., Piazza, M., Decesari, S., Gilardoni, S., Paglione, M., Cristofanelli, P., Marinoni, A., Bonasoni, P., and Belosi, F.: Atmospheric Ice Nucleating Particle measurements at the high mountain observatory Mt. Cimone (2165 m a.s.l., Italy), *Atmos. Environ.*, 171, 173–180, <https://doi.org/10.1016/j.atmosenv.2017.10.027>, 2017.

Schrod, J., Weber, D., Drücke, J., Kelehis, C., Pikridas, M., Ebert, M., Cvetković, B., Nickovic, S., Marinou, E., Baars, H., Ansmann, A., Vrekoussis, M., Mihalopoulos, N., Sciare, J., Curtius, J., and Bingemer, H. G.: Ice nucleating particles over the Eastern Mediterranean measured by unmanned aircraft systems, *Atmos. Chem. Phys.*, 17, 4817–4835, <https://doi.org/10.5194/acp-17-4817-2017>, 2017.

Schrod, J., Thomson, E. S., Weber, D., Kossmann, J., Pöhlker, C., Saturno, J., Ditas, F., Artaxo, P., Clouard, V., Saurel, J. M., Ebert, M., Curtius, J., and Bingemer, H. G.: Long-term deposition and condensation ice-nucleating particle measurements from four stations across the globe, *Atmos. Chem. Phys.*, 20, 15983–16006, <https://doi.org/10.5194/acp-20-15983-2020>, 2020.

Tobo, Y., Prenni, A. J., Demott, P. J., Huffman, J. A., McCluskey, C. S., Tian, G., Pöhlker, C., Pöschl, U., and Kreidenweis, S. M.: Biological aerosol particles as a key determinant of ice nuclei populations in a forest ecosystem, *J. Geophys. Res. Atmos.*, 118, 10,100–10,110, <https://doi.org/10.1002/jgrd.50801>, 2013.

Wang, B., Laskin, A., Roedel, T., Gilles, M. K., Moffet, R. C., Tivanski, A. V., and Knopf, D. A.: Heterogeneous ice nucleation and water uptake by field-collected atmospheric particles below 273 K, *J. Geophys. Res. Atmos.*, 117, 1–15, <https://doi.org/10.1029/2012JD017446>, 2012.

Welti, A., Müller, K., Fleming, Z. L., and Stratmann, F.: Concentration and variability of ice nuclei in the subtropical maritime boundary layer, 5307–5320, 2018.

Welti, A., Bigg, E. K., Demott, P. J., Gong, X., Hartmann, M., Harvey, M., Henning, S., Herenz, P., Hill, T. C. J., Hornblow, B., Leck, C., Löffler, M., Mccluskey, C. S., Rauker, A. M., Schmale, J., Tatzelt, C., and Pinxteren, M. Van: Ship-based measurements of ice nuclei concentrations over the Arctic , Atlantic , Pacific and Southern oceans, 15191–15206, 2020.

Wex, H., Huang, L., Zhang, W., Hung, H., Traversi, R., Becagli, S., Sheesley, R. J., Moffett, C. E., Barrett, T. E., Bossi, R., Skov, H., Hünerbein, A., Lubitz, J., Löffler, M., Linke, O., Hartmann, M., Herenz, P., and Stratmann, F.: Annual variability of ice-nucleating particle concentrations at different Arctic locations, *Atmos. Chem. Phys.*, 19, 5293–5311, <https://doi.org/10.5194/acp-19-5293-2019>, 2019.

Yin, J., Wang, D., and Guoqing, Z.: An Evaluation of Ice Nuclei Characteristics from the Long-term Measurement Data over North China An Evaluation of Ice Nuclei Characteristics from the Long-term Measurement Data over North China, <https://doi.org/10.1007/s13143-012-0020-8>, 2012.

Zuidema, P., Alvarez, C., Kramer, S. J., Custals, L., Izaguirre, M., Sealy, P., Prospero, J. M., and Blades, E.: Is summer African dust arriving earlier to Barbados?, *Bull. Am. Meteorol. Soc.*, 100, 1981–1986, <https://doi.org/10.1175/BAMS-D-18-0083.1>, 2019.